analytical chemistry

pubs.acs.org/ac

Article

Label-Free SERS for Rapid Differentiation of SARS-CoV-2-Induced Serum Metabolic Profiles in Non-Hospitalized Adults

Malama Chisanga, Hannah Williams, Denis Boudreau, Joelle N. Pelletier, Sylvie Trottier, and Jean-Francois Masson*

Cite This: *Anal. Chem.* 2023, 95, 3638−3646

Read Online

ACCESS | Metrics & More | Article Recommendations | Supporting Information

ABSTRACT: COVID-19 represents a multi-system infectious disease with broad-spectrum manifestations, including changes in host metabolic processes connected to the disease pathogenesis. Understanding biochemical dysregulation patterns as a consequence of COVID-19 illness promises to be crucial for tracking disease course and clinical outcomes. Surface-enhanced Raman scattering (SERS) has attracted considerable interest in biomedical diagnostics for the sensitive detection of intrinsic profiles of unique fingerprints of serum biomolecules indicative of SARS-CoV-2 infection in a label-free format. Here, we applied label-free SERS and chemometrics for rapid interrogation of temporal metabolic dynamics in longitudinal sera of mildly infected non-hospitalized patients (n = 22), at 4 and 16 weeks post PCR-positive diagnosis, and compared them with negative controls (n = 8). SERS spectral markers revealed distinct metabolic profiles in patient sera that significantly deviated from the healthy metabolic state at the two sampling time intervals. Multivariate and univariate analyses of the spectral data identified abundance dynamics in amino acids, lipids, and protein vibrations as the key spectral features underlying the metabolic differences detected in convalescent samples and perhaps associated with patient recovery progression. A validation study performed using spontaneous Raman spectroscopy yielded spectral data results that corroborated SERS spectral findings and confirmed the detected disease-specific molecular phenotypes in clinical samples. Label-free SERS promises to be a valuable analytical technique for rapid screening of the metabolic phenotype induced by SARS-CoV-2 infection to allow appropriate healthcare intervention.

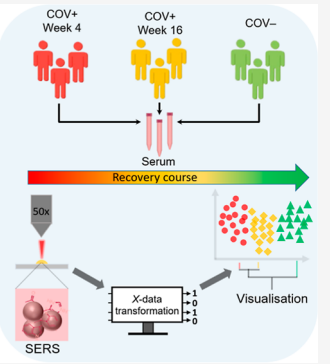

INTRODUCTION

COVID-19 infection caused by the coronavirus SARS-CoV-2 led to a global pandemic starting from the late 2019 stretching through 2022 and onward, posing a serious threat to healthcare systems. SARS-CoV-2 invades the respiratory tract, causing a systemic infection that may subsequently induce multi-organ inflammation or dysfunction in the host.[1] COVID-19 patients can be broadly classified from mild to severe cases depending on the clinical characteristics of COVID-19, with mild-to-moderate cases representing the vast majority of patients. Among patients who develop a mild illness, non-hospitalized subjects were often inadequately monitored post-infection, since the foremost aim of most studies was to unravel diagnostic and prognostic markers in severe and hospitalized patient cases who needed urgent attention. Given that most patients recover from the illness while a subset of patients develops severe disease, there is a strong interest in identifying biomarkers in COVID-19 patients that can predict disease severity and course, especially amidst increasing cases of long-COVID,[2] to guide healthcare decisions.

Molecular tests such as the PCR target the SARS-CoV-2 in active cases, while serological assays target immunoglobulins (IgG, IgM, and IgA) as biomarkers of current or past exposure to the virus, and these have been extensively used as gold standard diagnostic and screening tools for the SARS-CoV-2. However, the presence of the SARS-CoV-2 genome and/or protective antibodies does not reflect holistic biochemical changes as properties of pathogenesis and defence response,[3] nor inform on what set of biomolecular dynamics, in the wake of waning antibodies, are directly linked with patient recovery or mortality.[4]

Current studies have established a connection between COVID-19 and host metabolism and how this influences pathology over time. It is clear that infection-induced immune response stress exerts multiple changes in metabolic bioprocesses,[5] leading to metabolic dysregulation at various stages of the disease course and recovery phases. Increasing evidence shows that nearly 30% of patients experienced delayed recovery back to the healthy state after infection,[6] presenting an opportunity to examine the biochemical drivers of COVID-19 pathogenesis and recovery. Commonly dysregulated

Received: October 13, 2022
Accepted: January 31, 2023
Published: February 10, 2023

https://doi.org/10.1021/acs.analchem.2c04514
Anal. Chem. 2023, 95, 3638−3646

biomolecules implicated in COVID-19 which are detectable in patient biofluids (e.g., serum) include amino acids, lipoproteins, and lipids.[7,8] In this context, there is a paradigm shift toward measuring the "metabolic fingerprints" of patients as a platform for monitoring biochemical dysregulation profiles underlying pathophysiology and the immune response to SARS-CoV-2 infection.

Metabolomics based on mass spectrometry (MS) and NMR spectroscopy is well-suited for unravelling metabolic phenotypes, which can differentiate COVID-19 patients from healthy controls,[9] and identify potential molecular markers and mechanisms suggestive of COVID-19 course.[9,10] This is because the metabolome offers a holistic and functional snapshot of molecular profiles as the downstream product of the genome, transcriptome, and proteome influenced by the COVID-19 illness.[11] Several researchers have applied MS-based metabolomics to probe COVID-19 by monitoring circulating serum biomolecules. Roberts et al. used metabolic profiles and machine learning tools to predict COVID-19 severity and clinical outcomes based on the disease-modified levels of serum metabolites, including kynurenine, arginine, and uracil.[12] Similarly, Valdés et al. reported altered tryptophan, lipids, and purine metabolic pathways in patients 3 months post-infection with SARS-CoV-2 and classified early and end-stage COVID-19, including in patients with a mild infection.[13]

Although metabolomics studies have been demonstrated to provide valuable insights into the biomolecular mechanisms involved in COVID-19, sample preparation is time consuming and technically demanding. Ideally, initial screening of metabolic changes requires rapid, non-destructive, and less costly analytical tools that can quickly identify patient populations exhibiting molecular alterations in a biofluid such as plasma, which could then be further explored via metabolomics to identify differential metabolites.[14] There is also a need to develop a serum screening regimen that can confirm as well as complement MS to allow a comprehensive description of the metabolic properties of the SARS-CoV-2 infection. To this end, the aim of this study was to develop label-free surface-enhanced Raman scattering (SERS) as a metabolic fingerprinting technique for rapid analysis and differentiation of temporal metabolic changes in patients with mild COVID-19. This is especially desirable in cases, such as in the present study, where the volume of available clinical samples is too low (ca. 2−10 μL) for an MS-based omics study but adequately amenable to SERS clinical analysis.

Label-free SERS has attracted increasing attention in biomedical research as it can potentially fulfil the need to screen evolving disease states such as COVID-19,[15] in a rapid and reagent-free format with little or no sample handling. By combining molecularly specific information and intensified signals from molecules located within the electric fields generated by the surface plasmon on metallic nanoparticle (NP) surfaces,[16] SERS can achieve ultrasensitive detection of disease markers in the metabolome and other biopolymers with significantly reduced screening times.[17] A SERS spectrum of a liquid biopsy, such as serum, reveals distinct information-rich biomolecular fingerprints which, in the context of COVID-19 pathology and host response, represent the intrinsic metabolic states of interrogated patients. Any disease-specific perturbation in amino acids, carbohydrates, lipids, and proteins can be elucidated by SERS, with a view to being able to stratify between diseased patients and healthy controls.[14,15,18]

In the present study, for the first time, we used SERS and multivariate analysis for rapid characterization of biochemical composition and changes at 4 and 16 weeks post infection in PCR-verified non-hospitalized subjects with mild COVID-19. To complement and confirm SERS metabolic phenotypes, we applied spontaneous Raman spectroscopy to validate disease-specific changes in serum molecules, as shown previously for COVID-19 screening.[18,19] Raman spectroscopy extracts molecular information directly from polarizable chemical bonds of molecules without the need for extrinsic signal boosts such as NPs employed for SERS. In this regard, SERS and Raman spectroscopy can be considered complementary tools, providing confirmatory metabolic fingerprints associated with the disease course. Our conflated SERS and Raman platforms took advantage of simple sample handling steps, and rapid and non-invasive biosensing strategies, which are ideal for probing chemical trends in clinical samples. Significantly, spectral datasets revealed altered serum metabolic signatures in patients compared to the healthy controls. The detected biochemical shifts from the normal state led to the differentiation of patient sera collected longitudinally at weeks 4 and 16 post-infection, from healthy subjects, as revealed by multivariate analyses of spectral data.

EXPERIMENTAL METHODS

Synthesis of Silver NPs. All glassware used for metallic NP synthesis was thoroughly cleaned using aqua regia (3:1 hydrochloric acid/nitric acid) and copious amount of distilled water.

Silver NPs (AgNPs) were prepared via the reduction synthetic strategy reported previously.[20] Briefly, a 180 mL aqueous solution of 1.1 mM $AgNO_3$ was prepared in a 250 mL flask and uniformly mixed using a magnetic stirrer plate at room temperature in a fume hood. Next, 19 mL of an aqueous solution containing 1.88 mM hydroxylamine hydrochloride ($NH_2OH{\cdot}HCl$) and 3.33 mM NaOH was added dropwise to the $AgNO_3$ solution, resulting in color changes from a clear solution to a brown/orange color, indicating successful NP production. The colloid was stirred for a further 20 min before it was removed from the plate and stored at 4 °C. AgNP sol was characterized with UV−visible spectroscopy yielded a single surface plasmon band with an absorption maximum (λ_{max}) at 424 nm, while transmission emission microscopy (TEM) showed spherical AgNPs with an average diameter of ∼85 nm (Figure S1). AgNPs were concentrated 8× by centrifugation of the as-prepared colloid in 2 mL sterile vials at 11,000 rpm for 10 min. After discarding the supernatant, the pellets were reconstituted to the appropriate volume.

Clinical Samples. Participants with mild COVID-19 were randomly selected from the same cohort described previously.[21,22] All the volunteers were 18 years or older and had received a PCR-confirmed positive test for SARS-CoV-2 between 2 and 3 weeks prior to enrolment. Serum sampling was done at 4 and 16 weeks post-diagnosis. The mean age for patients (n = 22; 12 females, 10 males) and negative controls (n = 8; 7 females, 1 male) included in this study were 52.8 years (range: 20−78 years old) and 45.9 years (range: 20−55 years old), respectively. Negative controls were collected in June 2020 from subjects who had never received a COVID-positive test.

Sample Preparation. Thawed sera were aliquoted in triplicates and kept on ice throughout sample preparation protocols in a biosafety level 2 (BSL2) laboratory. Raw sera

https://doi.org/10.1021/acs.analchem.2c04514
Anal. Chem. 2023, 95, 3638−3646

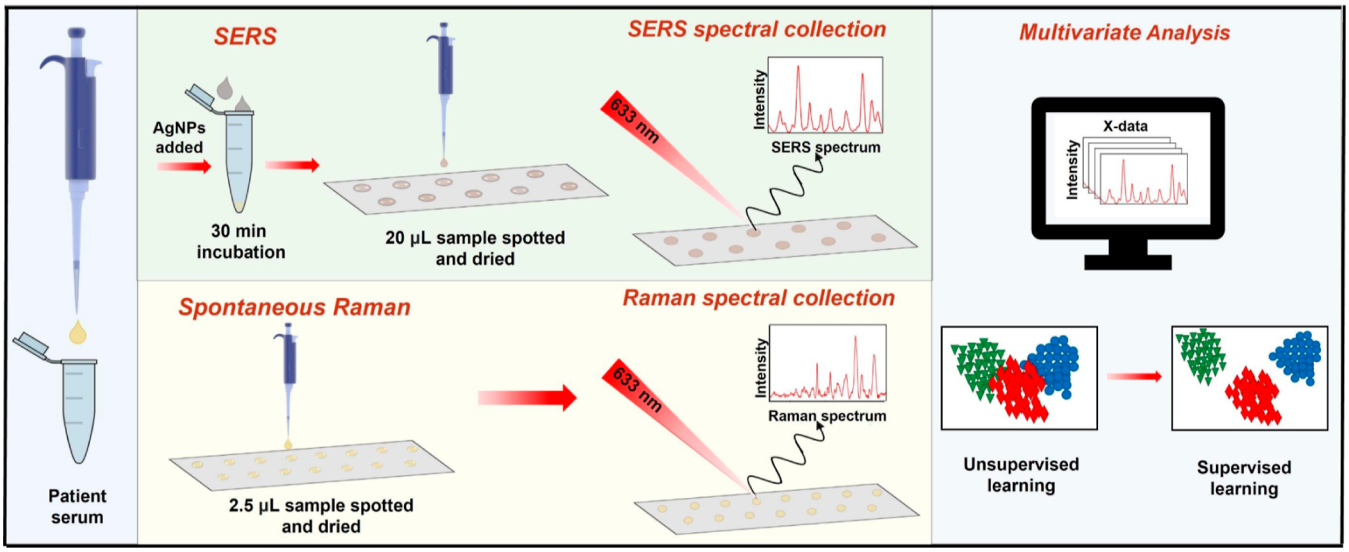

Figure 1. Illustration of the experimental design of the study: sample preparation and data acquisition protocols for label-free SERS and Raman analysis of sera. SERS spectral data were generated from sera incubated with AgNPs, while Raman signals were measured directly from samples after the drying step. Multivariate analysis was used to probe metabolic changes in sera.

were used without any sample processing to avoid losing important differential molecular markers in the samples, since processing of serum affects the biochemical content of serum.[23] For SERS, 10 μL of each sample was added to an equal volume of 8× concentrated AgNPs in an Eppendorf vial and mixed uniformly by vortexing. AgNPs-serum samples were incubated for 30 min, after which 20 μL of each sample was spotted onto aluminum foil-coated microscope slides and air-dried at room temperature. Prior to the experiment, a quality control (QC) sample was prepared by combining equal volumes of each of the patient samples, which was then used to assess the stability of AgNPs and SERS across 1 month. For spontaneous Raman spectroscopy, 2.5 μL of each clinical sample was drop-casted onto an aluminum foil-coated microscope slide and air-dried under the same conditions as the SERS protocols.

Spectral Data Acquisition. Both SERS and Raman spectra were acquired using an alpha300 confocal Raman microscope (WITec, Germany) equipped with a 633 nm HeNe excitation laser, a grating of 300 grooves/cm, and a CCD camera. A 50× magnifying objective was used to view the samples on aluminum foil-coated microscope glass slides and to collect the back-scattered photons. For SERS analysis, the laser power on the AgNPs-serum samples was adjusted to 40 mW with an exposure time of 5 s per signal. For Raman measurements, each dried sample was exposed to 40 mW for 90 s to acquire spectral data of good signal-to-noise ratio while preserving the biological integrity of sera. In all cases, three spectral signals were measured from randomly selected points of each of the three biological replicates prepared per sample. The Control 5 software was deployed for instrument control and data capture.

Data Processing and Chemometrics. Statistical analyses were performed in MATLAB software 2021b (The MathWorks Inc., Natwick, US) and GraphPad Prism. Spectra with obvious spurious spectral artefacts were considered outliers and removed from the dataset. All SERS and Raman spectral data were baseline corrected using the asymmetric least squares,[24] and scaled with the extended multiplicative signal correction,[25] before unsupervised principal component analysis (PCA) was applied. PCA was used to reduce the dimensionality of the data[26] and to explore natural clustering trends arising from COVID-19-specific metabolic changes in patients in comparison to negative controls. Both SERS and Raman datasets were further examined by a supervised model of principal component-canonical variates analysis (PC-CVA),[27] which minimized within-class variance while simultaneously maximizing between-class variance to differentiate samples according to a priori knowledge (patient groups).[28] PC-CVA was validated by generating a training set from 60% of randomly selected spectra from each patient group, which was then tested by projecting the remaining unseen 40% of the data into the subspace generated by the PC-CVA model.[29] To further simplify spectral interpretation, hierarchical cluster analysis (HCA) employing the Ward's linkage[30] was conducted on the PC-CVA scores per class to visualize separation distances among the patient classes. Pair-wise tests of statistical significance were conducted using two-tailed *t*-tests at the 95% confidence intervals. All statistical outputs were presented as averages of the spectral measurements, and the error bars represent the standard deviation of the mean.

RESULTS AND DISCUSSION

Figure 1 summarizes sample preparation protocols for SERS and spontaneous Raman spectral analyses, deploying simple steps amenable to clinical laboratories. The total spectral acquisition and data analysis time were 5 and 90 s per clinical sample for SERS and Raman spectroscopy, respectively.

As can be seen in Figure 1, the experimental designs for biomedical analysis of the serum metabolome were optimized for rapid analysis of sera using SERS and Raman spectroscopy. For SERS, serum was mixed in a 1:1 ratio with AgNPs, followed by an incubation time of 30 min, which allowed for sufficient interaction between serum biomolecules and the plasmonic particle surfaces. Reproducibility tests for AgNPs and SERS measured from a QC sample exhibited high stability and repeatability, as evidenced by the low relative standard deviations of 6.7% (0 weeks) and 5.6% (4 weeks), respectively (Figure S2). SERS and Raman spectral analyses were

https://doi.org/10.1021/acs.analchem.2c04514
Anal. Chem. 2023, 95, 3638−3646

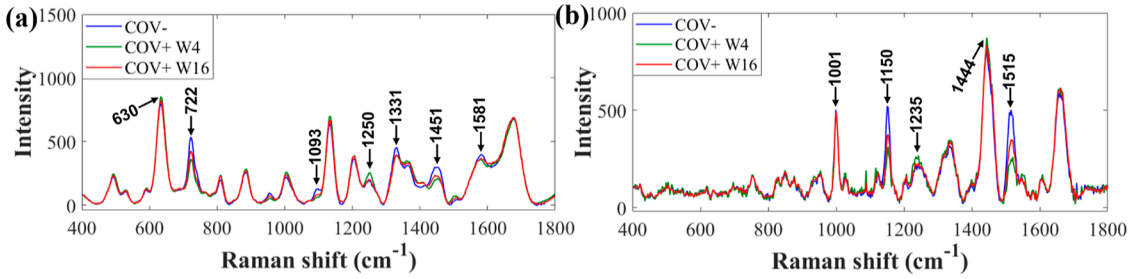

Figure 2. Averaged spectra for (a) SERS and (b) Raman spectroscopy measured from sera of negative controls (COV−, blue trace) and patients previously infected with SARS-CoV-2 (COV+) whose serum samples were collected after 4 weeks (COV+ W4, green trace) and 16 weeks (COV+ W16, red trace) post-diagnosis with SARS-CoV-2. Abbreviations; **W4**: 4 weeks, and **W16**: 16 weeks post-diagnosis. Annotated peaks highlight dominant discriminatory Raman shifts for respective serum samples.

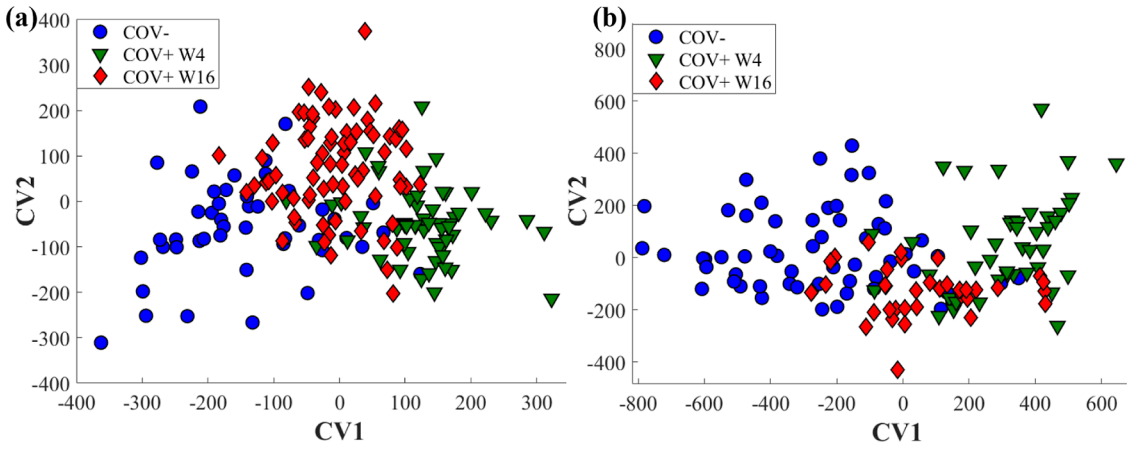

Figure 3. PC-CVA score biplots obtained by (a) SERS and (b) Raman spectral analysis of the sera from patients. Colored symbols represent different patient samples: blue spheres for negative controls (COV−), green triangles, and red diamonds for sera collected longitudinally at 4 weeks (COV+ W4) and 16 weeks (COV+ W16) post-infection.

performed on dried clinical samples under room temperature. It should also be noted that spectral data were processed in the same way and analyzed by unsupervised and supervised machine learning to guide fair comparison and validation of COVID-19-induced molecular dynamics unraveled by SERS and Raman spectral data, as illustrated in Figure 2.

Mean SERS and Raman spectra of sera from 22 non-hospitalized patients with mild COVID-19 (COV+), confirmed by PCR-positive nasopharyngeal swabs, and 8 negative control subjects who had never been diagnosed with COVID-19 (COV−) are shown in Figure 2. COV+ sera were collected longitudinally at weeks 4 (COV+ W4) and 16 (COV+ W16) post COVID-19 diagnosis had confirmed seroconversion of IgG at the tested time points, as we reported recently.[22] Sampling intervals of 4 and 16 weeks post-diagnosis were investigated, as they represent an estimate of peak immune response and recovery time points, respectively, following the onset of SARS-CoV-2 infection.[31] The spectra for COV+ and COV− sera exhibited a high degree of similarity; however, closer inspection and statistical analysis of the spectra revealed metabolite peaks of varying abundances in clinical samples. The next step was therefore to determine whether the SERS and Raman fingerprints for the COV+ and COV− sera were sufficient to differentiate and group the investigated subjects according to their expected clinical states [i.e., COV+ (longitudinal sera at week 4 and week 16 post-diagnosis) and COV− (sera from negative controls)].

SERS Spectral Analysis. PC-CVA scores of the SERS spectral data shown in Figure 3a displayed separations between patient sera collected at weeks 4 and 16 post-diagnosis (COV+) and negative control sera (COV−) as dominant variables along the CV1 axis.

Corresponding PCA score biplots are shown in Figure S3a. Though sera of COV+ patients clustered closely and away from COV− samples, it appeared that COV+ sera collected at week 4 clustered further away from COV− samples, while week 16 sera clustered between the extreme COV− and COV+ week 4 samples along CV1. This suggests significantly changed metabolic profiles in COV+ patients 4 weeks post-diagnosis of SARS-CoV-2 compared to COV− sera. By contrast, week 16 patient sera appeared to exhibit intermediate metabolic alterations between those for week 4 and COV− subjects, which is also indicative of persistent biochemical pathophysiology as well as progressive recovery from mild illness, moving toward the healthy metabolic status. The differences seen among the three investigated groups originated mainly from adenine and adenine-related compounds, proteins, lipids, and amino acids. This observation is consistent with recent findings reported by Valdés and co-workers, where longitudinal sera collected 2−3 months apart, from hospitalized mild COV+, had distinctive metabolic differences in proteins, lipids and a host of metabolites unraveled via PCA and PLS-DA.[13] Contrary to CV1, CV2 attempted to separate COV+ W16 from the other patient categories (Figure 3a). PC-CVA was validated by the projection method that showed congruent clusters of the training and test spectral datasets used for model validation (Figure S4), demonstrating reproducible classification solely

https://doi.org/10.1021/acs.analchem.2c04514
Anal. Chem. 2023, 95, 3638−3646

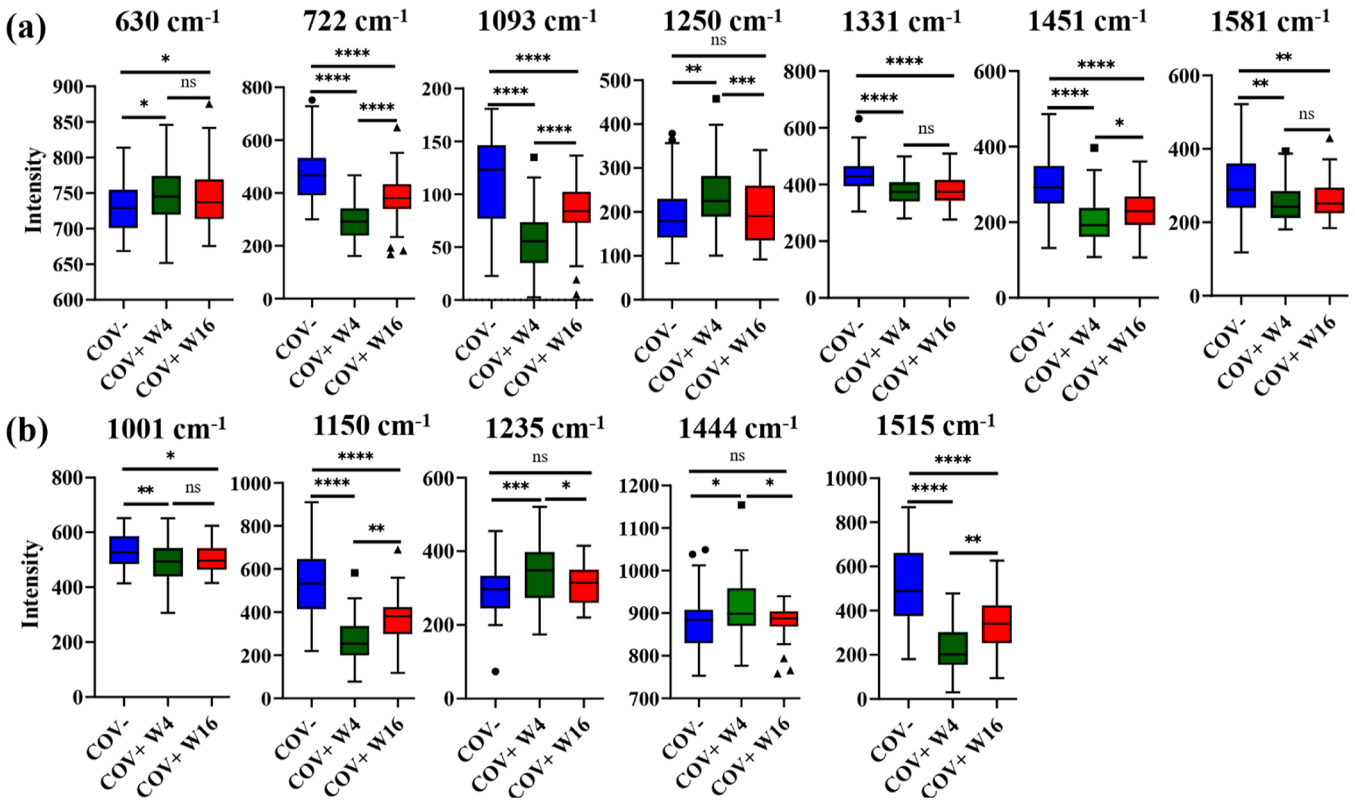

Figure 4. Boxplots generated from peak analysis of prominent spectral biomarkers identified using (a) SERS and (b) Raman spectroscopy showing chemical trends associated with COVID-19 at weeks 4 (COV+ W4, green trace) and 16 (COV+ W16, red trace) compared to controls (COV−, blue trace). Number annotations above the boxplots represent Raman shifts for the main spectral intensities at: (a) 630, 722, 1093, and 1331 (hypoxanthine), 1230−1250 (amide III), 1440−1451 (lipids/proteins), and 1581 cm^{-1} (proteins), (b) 1001 (phenylalanine), 1150 (proteins), and 1515 cm^{-1} (carotenoids). ****$p < 0.0001$, ***$p < 0.001$, **$p < 0.01$, *$p < 0.05$, **ns**: not significant, based on two-tailed *t*-tests of each two-group comparison. The whiskers extend to the most extreme data points which are not considered outliers (shown), defined as no more than 1.5 × IQR outside of the IQR.

representative of the metabolic changes in the tested sera and not artefacts from the statistical model. In order to rationalize the molecular-level origin of the clustering trends detected in Figure 3, we plotted CVA loadings to be able to identify key classes of biomolecules and associated abundance dynamics related to COVID-19.

According to the CV loadings (Figure S5a), the major explanatory SERS vibrational modes attributed to the separations observed on CVA scores (Figure 3a) displayed intensity differences that corresponded to metabolites present in higher or lower relative levels in patient sera. The dominant peaks at 722, 1093, and 1331 cm^{-1} (ring modes in hypoxanthine/purines and analogues),[32−35] and bands at 1451 cm^{-1} (CH_2 deformations in lipids/proteins) and 1581 cm^{-1} (ring modes in amino acids),[36,37] as shown in Table S1, were detected in higher quantities in the sera of COV− than COV+ patients group (Figure 3a), indicating metabolite downregulation in response to SARS-CoV-2 infection and recovery. On the other hand, the main characteristic bands detected at 630 cm^{-1} (uric acid) and 1250 cm^{-1} (amide III vibration),[34,36] were present in greater amounts in the sera of COV+ patients than COV− subjects (Figure 2a), suggesting upregulation of biomolecules in COV+ groups.

The concentration patterns in major serum metabolites underlying metabolic changes in COV+ patients (as highlighted by CV loadings and CVA score plots) are summarized in the form of boxplots as shown in Figures 4a and S6. In general, a V-shaped trajectory of serum metabolite changes is observed; that is, the intensities of the significantly changing spectral bands of COV+ sera which initially varied in intensity (increased or decreased) in COV+ sera at week 4, tended to shift toward the initial intensity 16 weeks after infection, suggesting partial reversion of metabolic states back to the healthy metabolic phenotype. Specifically, the SERS spectral bands at 722, 1093, and 1451 cm^{-1}, which initially decreased significantly in COV+ sera at week 4, significantly increased in intensity 16 weeks. The amide III peak at 1250 cm^{-1} showed an opposite trend, where metabolites increased at week 4 before drifting back to the baseline (COV−) at week 16, again consistent with the probable phenoreversion of COV+ to a normal metabolic state.[38] V-shaped trends of lesser significance were similarly observed for the other spectral bands identified in Figures 4a and S6.

Major metabolites (hypoxanthine, uric acid, and lipids) assigned to the differential spectral markers are associated with SARS-CoV-2 infection,[39,40] and have been utilized to discriminate between mild COV+ and healthy adults.[8,41] Some authors have also explored the evolution of metabolic features at different time intervals post-symptom onset as correlates of COVID-19 pathogenesis and immune response.[42] Recently, machine learning-aided metabolomics revealed COVID-19-specific trends of dysregulation, similar to those reported in the present work, in various classes of biological compounds, including lipids (1450 cm^{-1}), proteins (1250 cm^{-1}), amino acids (630, 1093 cm^{-1}), and adenine and its derivatives, such as methyladenosine, in mildly infected

https://doi.org/10.1021/acs.analchem.2c04514
Anal. Chem. 2023, 95, 3638−3646

patients.[13,43] The levels of metabolic components decreased in the longitudinal plasma of the COV+ after ∼3 weeks post-symptom onset, before rising gradually, reaching a similar metabolic state to that detected for the COV− subjects 14 weeks post-infection,[43] which is in agreement with the probable metabolic healing process of COV+ patients observed in our results presented in Figure 4a. Recent studies show that SARS-CoV-2 infection alters several metabolic pathways, such as the kynurenine, lipid, and tryptophan pathway,[12] which explains the upregulation and downregulation of amino acids, lipids, and proteins spectral modes associated with clustering trends in CVA scores. Among the discriminating compounds detected previously, and also reported in this study, were biomolecular dynamics (e.g., uric acid) that are known to be indicative of dysregulated purine,[12] and lipid,[39] metabolic pathways induced by COVID-19 persisting for up to 10 months in some patients post-infection. Hence, the dominant SERS spectral markers detected in this study highlighted both time-dependent systematic metabolic trends in COV+ and recovery in patients who had mild COVID-19 illness relative to negative control sera. This offers clinically vital molecular information that may predict patient outcomes.

To explore serum molecular phenotypes even further, HCA plots were constructed from mean PC-CVA scores. Figure S7a shows a dendrogram for HCA of SERS data identifying two metabolically distinct classes of clinical samples, where COV− clustered far away from COV+. It is also evident from HCA trees that even though the samples from weeks 4 and 16 formed a unique cluster by virtue of exhibiting similar metabolic trends (both are COV+), week 16 serum samples clustered in the middle, closer to both COV− and COV+ week 4 groups than do the COV− and COV+ week 4 groups (Figure S7a). This observation was also consistent with the PC-CVA finding of the SERS data (Figure 3a) discussed above.

Raman Spectral Analysis. Unsupervised analysis of the Raman spectral data by PC-CVA (Figure 3b) and PCA (Figure S3b) scores exhibited similar clustering trends to those observed for the SERS data (Figure 3a). According to CV1 in Figure 3b, COV− samples clustered far left from the COV+ week 4 samples located on the far right, with COV+ week 16 sera positioned between COV− and COV+ week 4. Clear overlaps seen among the scores for COV− and COV+ (weeks 4 and 16) are thought to reflect progressive recovery and reversion of metabolic phenotypes in the patients 16 weeks after the SARS-CoV-2 diagnosis detected by SERS. Like the SERS data, CV2 of the Raman data attempted to differentiate COV+ W4 from the rest of the clinical samples.

Inspection of the CV1 loadings (Figure S5b) of the Raman data indicated nearly identical spectral trends for COV+ and COV−, except mainly for the vibrational modes at 1150 cm^{-1} (C−N stretch in proteins) and 1515 cm^{-1} (carotenoids),[44,45] (Figure 2b), that were the salient spectral features associated with PC-CVA scores in Figure 3b. Further analysis of CV loadings plots characteristic bands unraveled serum biochemical dysregulation dynamics similar to the SERS bands (Figure 2a), where the spectral features (mainly proteins and amino acids, Table S2)[45] exhibited higher relative amounts in COV− than COV+ sera (Figure 2b), in line with molecular trends observed recently in COVID-19 patients via Raman spectroscopy.[46] This finding was further supported by proteomics studies that also reported significantly raised protein levels in mild-to-moderately infected COV+ patients relative to healthy controls.[47] In addition, COV+ displayed major variations in proteins at week 16, following a dip in these molecules at week 4, as indicated on Figure 4b. In contrast, phenylalanine and tryptophan[48] were downregulated in COV+ as shown by the phenylalanine/tryptophan Raman biomarker band detected at 1001 cm^{-1} (Figure 4b), whose intensity decreased in COV+ compared to COV− sera.[48,49] These observations complement and confirm SERS spectral findings, illustrating the robustness and reproducibility of our SERS protocol.

The HCA dendrogram computed from PC-CVA scores of Raman data also revealed clustering profiles of the samples where the COV− were separated from COV+ sera (Figure S7b), reflecting differentially expressed metabolic responses to SARS-CoV-2 viral infection in COV+ patients unlike in the COV− individuals. Despite having altered metabolism, the COV+ week 16 clustered much closer to the COV− than the COV+ week 4 samples were to the COV− (Figure 3b), which again may be indicative of time-course recovery phases post-infection seen in the SERS data (Figure 3a).

At this stage, it is very clear that the SERS and Raman data demonstrated very similar metabolic profiles in COV+ and COV− subjects, though the spectral features dictating the metabolic trends in the samples originated from different molecular vibrations (mainly hypoxanthine/amino acids, uric acid, lipids, and amides for SERS; mainly proteins for Raman). This finding is perhaps not surprising given that the two metabolic fingerprinting tools yield confirmatory and complementary serum molecular information, as shown previously for cancer diagnostics/screening.[50] More importantly, SERS and Raman spectral data reported in the present study have demonstrated consistent differential metabolic patterns of acceptable reproducibility for COV+ and COV− individuals. It should also be emphasized that the patients tested in this study were infected early in the COVID-19 pandemic before SARS-CoV-2 variants emerged and infected humans,[22] such that the variabilities in metabolic phenotypes detected by SERS and Raman spectroscopic tools were unlikely to be influenced by infection with different SARS-CoV-2 variants.

While the results discussed above have offered informative insights into metabolic changes related to COVID-19 and corresponding time course recovery post infection, there are some limitations in this study. First of all, the small sample size (n = 30) and few sampling points limited the extrapolation of our results to a larger population. Expanding the spectral datasets by enrolling more patients would not only lead to a better representation of the findings but would also boost the statistical power of machine learning tools. Second, patient health records, such as lifestyle and comorbidities, that can influence variability in the data were not available at the time of serum sampling. Nonetheless, the investigated longitudinal sera were collected from the same patient cohort (n = 22) at weeks 4 and 16 time points, and this may have reduced spurious spectral variations. In addition, the difference in average age for the COV+ (52.8 years old) and the COV− (45.9 years old) was not statistically significant (p = 0.3179) (Figure S8), indicating matched patient age, and this reduced age-related chemical trends. We also noted that, unlike in COV+ groups where patient gender was fairly paired, COV− category was dominated by females, reflecting a disproportionate and partial representation of COVID-19-specific metabolic changes. Efforts to acquire metadata for COV+ patients and to balance gender in the COV− group proved futile, as this was beyond the scope of the study. However,

https://doi.org/10.1021/acs.analchem.2c04514
Anal. Chem. 2023, 95, 3638−3646

given that this is the first study to demonstrate the applicability of SERS and Raman spectroscopy combined with chemometrics to investigate SARS-CoV-2-induced chemical phenotype, the reported spectroscopic profiles from mildly infected COVID-19 patients will act as a foundation upon which future studies will be built.

CONCLUSIONS

We have demonstrated that COVID-19-induced metabolic changes measured by SERS combined with chemometrics can rapidly differentiate convalescent patients from negative controls. The SERS spectral fingerprints revealed that non-hospitalized patients with mild COVID-19 exhibited altered metabolic profiles at weeks 4 and 16 post SARS-CoV-2 diagnosis that were significantly different from healthy negative controls. Interestingly, the metabolic changes of week 16 sera suggested progressive recovery of patients detected intermediate between the COV+ week 4 and COV− sera, with main differential molecular changes identified in amino acids, lipids, and proteins. Raman spectroscopic analysis of the molecular profiles of patients validated the differential SERS spectral markers, that provided further evidence that COVID-19 affected the levels of circulating metabolites and biopolymers in patient samples. We envisage that when structural resolution and elucidation of spectral marker metabolites are achieved and validated via MS or NMR metabolomics strategies, targeted SERS may play an important role in absolute quantitative detection of single and multiple COVID-19 molecular markers,[14] aimed at predicting quantitative severity (mild or severe) and clinical outcomes of SARS-CoV-2 viral infection potentially at the point of use. It also remains to be seen if these changes are specific to the SARS-CoV-2 infection or if they represent a nonspecific metabolic response than could also apply to other infection processes.

ASSOCIATED CONTENT

Supporting Information

The Supporting Information is available free of charge at https://pubs.acs.org/doi/10.1021/acs.analchem.2c04514.

Extra details of NP characterization techniques, NP stability tests, machine learning validation, CV loadings, boxplots for low intensity bands, HCA of spectral data, tentative spectral band assignments, and statistical comparison of patient age dynamics (PDF)

AUTHOR INFORMATION

Corresponding Author

Jean-Francois Masson − *Department of Chemistry, Québec Centre for Advanced Materials (QCAM), Regroupement Québécois sur les Matériaux de Pointe (RQMP), and Centre Interdisciplinaire de Recherche sur le Cerveau et l'Apprentissage (CIRCA), Université de Montréal, Montreal, Québec H3C 3J7, Canada;* orcid.org/0000-0002-0101-0468; Phone: +1-514-343-7342; Email: jf.masson@umontreal.ca

Authors

Malama Chisanga − *Department of Chemistry, Québec Centre for Advanced Materials (QCAM), Regroupement Québécois sur les Matériaux de Pointe (RQMP), and Centre Interdisciplinaire de Recherche sur le Cerveau et l'Apprentissage (CIRCA), Université de Montréal, Montreal, Québec H3C 3J7, Canada;* orcid.org/0000-0002-1481-1299

Hannah Williams − *Department of Chemistry, Québec Centre for Advanced Materials (QCAM), Regroupement Québécois sur les Matériaux de Pointe (RQMP), and Centre Interdisciplinaire de Recherche sur le Cerveau et l'Apprentissage (CIRCA), Université de Montréal, Montreal, Québec H3C 3J7, Canada*

Denis Boudreau − *Department of Chemistry and Centre for Optics, Photonics and Lasers (COPL), Université Laval, Québec, Québec G1V 0A6, Canada;* orcid.org/0000-0001-5152-2464

Joelle N. Pelletier − *Department of Chemistry, Department of Biochemistry and PROTEO, Québec Network for Research on Protein Function, Engineering and Applications, Université de Montréal, Montreal, Québec H3C 3J7, Canada;* orcid.org/0000-0002-2934-6940

Sylvie Trottier − *Centre de Recherche du Centre Hospitalier Universitaire de Québec and Département de Microbiologie-Infectiologie et d'Immunologie, Université Laval, Québec, Québec G1V 4G2, Canada;* orcid.org/0000-0002-3986-5146

Complete contact information is available at: https://pubs.acs.org/10.1021/acs.analchem.2c04514

Author Contributions

Conceptualization: M.C. and J.-F.M. methodology: M.C., H.W., S.T., and J.-F.M. investigation: M.C. and H.W. data acquisition and analysis: M.C. and H.W. writing original draft: M.C. supervision: D.B., J.N.P., and J.-F.M. funding: D.B., J.N.P., S.T., and J.-F.M. The final article was revised and approved by all the authors.

Notes

The authors declare no competing financial interest.

ACKNOWLEDGMENTS

We acknowledge financial support from the Canadian Institutes of Health Research (CIHR), the Natural Sciences and Engineering Research Council of Canada (NSERC), the Pandemic Response Challenge Program of the National Research Council Canada, and the Canadian Foundation for Innovation (CFI).

REFERENCES

(1) Nie, X.; Qian, L. J.; Sun, R.; Huang, B.; Dong, X. C.; Xiao, Q.; Zhang, Q. S.; Lu, T.; Yue, L.; Chen, S.; Li, X.; Sun, Y. T.; Li, L.; Xu, L.; Li, Y.; Yang, M.; Xue, Z. Z.; Liang, S.; Ding, X.; Yuan, C. H.; Peng, L.; Liu, W.; Yi, X.; Lyu, M. G.; Xiao, G. X.; Xu, X.; Ge, W. G.; He, J. L.; Fan, J.; Wu, J. H.; Luo, M.; Chang, X. N.; Pan, H. X.; Cai, X.; Zhou, J. J.; Yu, J.; Gao, H. H.; Xie, M. X.; Wang, S. H.; Ruan, G.; Chen, H.; Su, H.; Mei, H.; Luo, D. J.; Zhao, D. S.; Xu, F.; Li, Y.; Zhu, Y.; Xia, J.; Hu, Y.; Guo, T. *Cell* **2021**, *184*, 775−791.

(2) Nalbandian, A.; Sehgal, K.; Gupta, A.; Madhavan, M. V.; McGroder, C.; Stevens, J. S.; Cook, J. R.; Nordvig, A. S.; Shalev, D.; Sehrawat, T. S.; Ahluwalia, N.; Bikdeli, B.; Dietz, D.; Der-Nigoghossian, C.; Liyanage-Don, N.; Rosner, G. F.; Bernstein, E. J.; Mohan, S.; Beckley, A. A.; Seres, D. S.; Choueiri, T. K.; Uriel, N.; Ausiello, J. C.; Accili, D.; Freedberg, D. E.; Baldwin, M.; Schwartz, A.; Brodie, D.; Garcia, C. K.; Elkind, M. S. V.; Connors, J. M.; Bilezikian, J. P.; Landry, D. W.; Wan, E. E. Y. *Nat. Med.* **2021**, *27*, 601−615.

(3) López-Hernández, Y.; Monárrez-Espino, J.; Oostdam, A. S.; Delgado, J. E. C.; Zhang, L.; Zheng, J. M.; Valdez, J. J. O.; Mandal, R.; González, F. D. O.; Moreno, J. C. B.; Trejo-Medinilla, F. M.; López, J. A.; Moreno, J. A. E.; Wishart, D. S. *Sci. Rep.* **2021**, *11*, 14732−14744.

(4) Marín-Corral, J.; Rodríguez-Morató, J.; Gomez-Gomez, A.; Pascual-Guardia, S.; Muñoz-Bermúdez, R.; Salazar-Degracia, A.; Pérez-Terán, P.; Restrepo, M. I.; Khymenets, O.; Haro, N.; Masclans, J. R.; Pozo, O. J. *Int. J. Mol. Sci.* **2021**, *22*, 4794−4807.
(5) Xiao, N.; Nie, M.; Pang, H. H.; Wang, B. H.; Hu, J. L.; Meng, X. J.; Li, K.; Ran, X. R.; Long, Q. X.; Deng, H. J.; Chen, N.; Li, S.; Tang, N.; Huang, A. L.; Hu, Z. P. *Nat. Commun.* **2021**, *12*, 1618−1630.
(6) Ayres, J. S. *Nat. Metab.* **2020**, *2*, 572−585.
(7) Thomas, T.; Stefanoni, D.; Reisz, J. A.; Nemkov, T.; Bertolone, L.; Francis, R. O.; Hudson, K. E.; Zimring, J. C.; Hansen, K. C.; Hod, E. A.; Spitalnik, S. L.; D'Alessandro, A. *JCI Insight* **2020**, *5*, e140327−e140342.
(8) Páez-Franco, J. C.; Torres-Ruiz, J.; Sosa-Hernández, V. A.; Cervantes-Díaz, R.; Romero-Ramírez, S.; Pérez-Fragoso, A.; Meza-Sánchez, D. E.; Germán-Acacio, J. M.; Maravillas-Montero, J. L.; Mejía-Domínguez, N. R.; Ponce-de-León, A.; Ulloa-Aguirre, A.; Gómez-Martín, D.; Llorente, L. *Sci. Rep.* **2021**, *11*, 6350−6361.
(9) Pang, Z. Q.; Zhou, G. Y.; Chong, J.; Xia, J. G. *Metabolites* **2021**, *11*, 44−57.
(10) Barberis, E.; Amede, E.; Khoso, S.; Castello, L.; Sainaghi, P. P.; Bellan, M.; Balbo, P. E.; Patti, G.; Brustia, D.; Giordano, M.; Rolla, R.; Chiocchetti, A.; Romani, G.; Manfredi, M.; Vaschetto, R. *Metabolites* **2021**, *11*, 847−857.
(11) Chen, Y. M.; Zheng, Y. T.; Yu, Y.; Wang, Y. Z.; Huang, Q. X.; Qian, F.; Sun, L.; Song, Z. G.; Chen, Z. Y.; Feng, J. W.; An, Y. P.; Yang, J. C.; Su, Z. Q.; Sun, S. Y.; Dai, F. H.; Chen, Q. S.; Lu, Q. W.; Li, P. C.; Ling, Y.; Yang, Z.; Tang, H. R.; Shi, L. M.; Jin, L.; Holmes, E. C.; Ding, C.; Zhu, T. Y.; Zhang, Y. Z. *EMBO J.* **2020**, *39*, e105896−e105918.
(12) Roberts, I.; Muelas, M. W.; Taylor, J. M.; Davison, A. S.; Xu, Y.; Grixti, J. M.; Gotts, N.; Sorokin, A.; Goodacre, R.; Kell, D. B. *Metabolomics* **2022**, *18*, 6−24.
(13) Valdés, A.; Moreno, L. O.; Rello, S. R.; Orduña, A.; Bernardo, D.; Cifuentes, A. *Sci. Rep.* **2022**, *12*, 1650−1660.
(14) Chisanga, M.; Muhamadali, H.; Ellis, D. I.; Goodacre, R. *Appl. Sci.* **2019**, *9*, 1163−1186.
(15) Paria, D.; Kwok, K. S.; Raj, P.; Zheng, P.; Gracias, D. H.; Barman, I. *Nano Lett.* **2022**, *22*, 3620−3627.
(16) Langer, J.; de Aberasturi, D. J.; Aizpurua, J.; Alvarez-Puebla, R. A.; Auguie, B.; Baumberg, J. J.; Bazan, G. C.; Bell, S. E. J.; Boisen, A.; Brolo, A. G.; Choo, J.; Cialla-May, D.; Deckert, V.; Fabris, L.; Faulds, K.; de Abajo, F. J. G.; Goodacre, R.; Graham, D.; Haes, A. J.; Haynes, C. L.; Huck, C.; Itoh, T.; Ka, M.; Kneipp, J.; Kotov, N. A.; Kuang, H.; Le Ru, E. C.; Lee, H. K.; Li, J. F.; Ling, X. Y.; Maier, S. A.; Mayerhofer, T.; Moskovits, M.; Murakoshi, K.; Nam, J. M.; Nie, S.; Ozaki, Y.; Pastoriza-Santos, I.; Perez-Juste, J.; Popp, J.; Pucci, A.; Reich, S.; Ren, B.; Schatz, G. C.; Shegai, T.; Schlucker, S.; Tay, L. L.; Thomas, K. G.; Tian, Z. Q.; Van Duyne, R. P.; Vo-Dinh, T.; Wang, Y.; Willets, K. A.; Xu, C.; Xu, H.; Xu, Y.; Yamamoto, Y. S.; Zhao, B.; Liz-Marzan, L. M. *ACS Nano* **2020**, *14*, 28−117.
(17) Aizpurua, J.; Arnolds, H.; Baumberg, J.; Bruzas, I.; Chikkaraddy, R.; Chisanga, M.; Dawson, P.; Deckert, V.; Delfino, I.; de Nijs, B.; Di Martino, G.; Edel, J.; Fleming, H.; Gawinkowski, S.; Giorgis, F.; Goodacre, R.; Graham, D.; Hardy, M.; Heck, C.; Heeg, S.; Hewitt, K.; Jamieson, L.; Keeler, A.; Królikowska, A.; Kuttner, C.; Lidgi-Guigui, N.; Lightner, C.; Lombardi, J.; Mahajan, S.; Martín Sabanés, N. M.; Masson, J. F.; Mueller, N. S.; Muhamadali, H.; Murakoshi, K.; Popp, J.; Porter, M.; Reich, S.; Schatz, G.; Tian, Z. Q.; Tripathi, A.; Van Duyne, R.; Wang, X. P.; Wark, A.; Willets, K.; Willner, M. *Faraday Discuss.* **2017**, *205*, 291−330.
(18) Carlomagno, C.; Bertazioli, D.; Gualerzi, A.; Picciolini, S.; Banfi, P. I.; Lax, A.; Messina, E.; Navarro, J.; Bianchi, L.; Caronni, A.; Marenco, F.; Monteleone, S.; Arienti, C.; Bedoni, M. *Sci. Rep.* **2021**, *11*, 4943−4955.
(19) Yin, G.; Li, L. T.; Lu, S.; Yin, Y.; Su, Y. Z.; Zeng, Y. L.; Luo, M.; Ma, M. H.; Zhou, H. Y.; Orlandini, L.; Yao, D. Z.; Liu, G.; Lang, J. Y. *J. Raman Spectrosc.* **2021**, *52*, 949−958.
(20) Leopold, N.; Lendl, B. *J. Phys. Chem. B* **2003**, *107*, 5723−5727.
(21) Chisanga, M.; Stuible, M.; Gervais, C.; L'Abbé, D.; Cass, B.; Bisson, L.; Pelletier, A.; Lord-Dufour, S.; Durocher, Y.; Boudreau, D.; Trottier, S.; Pelletier, J. N.; Masson, J.-F. *Sens. Diagn.* **2022**, *1*, 851−866.
(22) Jodaylami, M. H.; Djaileb, A.; Ricard, P.; Lavallee, E.; Cellier-Goethebeur, S.; Parker, M. F.; Coutu, J.; Stuible, M.; Gervais, C.; Durocher, Y.; Desautels, F.; Cayer, M. P.; de Grandmont, M. J.; Rochette, S.; Brouard, D.; Trottier, S.; Boudreau, D.; Pelletier, J. N.; Masson, J. F. *Sci. Rep.* **2021**, *11*, 21601−21611.
(23) Avci, E.; Yilmaz, H.; Sahiner, N.; Tuna, B. G.; Cicekdal, M. B.; Eser, M.; Basak, K.; Altıntoprak, F.; Zengin, I.; Dogan, S.; Çulha, M. *Cancers* **2022**, *14*, 5021−5035.
(24) Eilers, P. H. C. *Anal. Chem.* **2004**, *76*, 404−411.
(25) Afseth, N. K.; Kohler, A. *Chemom. Intell. Lab. Syst.* **2012**, *117*, 92−99.
(26) Brereton, R. G. *J. Chemom.* **2022**, *36*, e3405−e3408.
(27) Gromski, P. S.; Muhamadali, H.; Ellis, D. I.; Xu, Y.; Correa, E.; Turner, M. L.; Goodacre, R. *Anal. Chim. Acta* **2015**, *879*, 10−23.
(28) Goodacre, R. *Vib. Spectrosc.* **2003**, *32*, 33−45.
(29) Radovic, B. S.; Goodacre, R.; Anklam, E. *J. Anal. Appl. Pyrolysis* **2001**, *60*, 79−87.
(30) Chisanga, M.; Linton, D.; Muhamadali, H.; Ellis, D. I.; Kimber, R. L.; Mironov, A.; Goodacre, R. *Analyst* **2020**, *145*, 1236−1249.
(31) Wang, Y. Q.; Zhang, L.; Sang, L.; Ye, F.; Ruan, S. C.; Zhong, B.; Song, T.; Alshukairi, A. N.; Chen, R. C.; Zhang, Z. Y.; Gan, M.; Zhu, A. R.; Huang, Y. B.; Luo, L.; Mok, C. K. P.; Al Gethamy, M. M.; Tan, H. T.; Li, Z. T.; Huang, X. F.; Li, F.; Sun, J.; Zhang, Y. J.; Wen, L. Y.; Li, Y. M.; Chen, Z.; Zhuang, Z.; Zhuo, J. F.; Chen, C. K.; Kuang, L. J.; Wang, J. X.; Lv, H. B.; Jiang, Y. L.; Li, M.; Lin, Y. M.; Deng, Y.; Tang, L.; Liang, J. L.; Huang, J. C.; Perlman, S.; Zhong, N. S.; Zhao, J. X.; Peiris, J. S. M.; Li, Y. M.; Zhao, J. C. *J. Clin. Invest.* **2020**, *130*, 5235−5244.
(32) Moisoiu, T.; Iancu, S. D.; Burghelea, D.; Dragomir, M. P.; Iacob, G.; Stefancu, A.; Cozan, R. G.; Antal, O.; Bálint, Z.; Muntean, V.; Badea, R. I.; Licarete, E.; Leopold, N.; Elec, F. I. *Biomedicines* **2022**, *10*, 233−241.
(33) Cervo, S.; Mansutti, E.; Del Mistro, G.; Spizzo, R.; Colombatti, A.; Steffan, A.; Sergo, V.; Bonifacio, A. *Anal. Bioanal. Chem.* **2015**, *407*, 7503−7509.
(34) Stefancu, A.; Moisoiu, V.; Couti, R.; Andras, I.; Rahota, R.; Crisan, D.; Pavel, I. E.; Socaciu, C.; Leopold, N.; Crisan, N. *Nanomedicine* **2018**, *13*, 2455−2467.
(35) Balaikaite, A.; Chisanga, M.; Fisher, K.; Heyes, D. J.; Spiess, R.; Leys, D. *ACS Chem. Biol.* **2020**, *15*, 2466−2475.
(36) Esposito, A.; Bonifacio, A.; Sergo, V.; Fornasaro, S. *Biosensors* **2021**, *11*, 467−478.
(37) Wang, J.; Lin, D.; Lin, J. Q.; Yu, Y.; Huang, Z. F.; Chen, Y. P.; Lin, J. Y.; Feng, S. Y.; Li, B. H.; Liu, N. R.; Chen, R. *J. Biomed. Opt.* **2014**, *19*, 087003−087011.
(38) Holmes, E.; Wist, J.; Masuda, R.; Lodge, S.; Nitschke, P.; Kimhofer, T.; Loo, R. L.; Begum, S.; Boughton, B.; Yang, R. C.; Morillon, A. C.; Chin, S. T.; Hall, D.; Ryan, M.; Bong, S. H.; Gay, M.; Edgar, D. W.; Lindon, J. C.; Richards, T.; Yeap, B. B.; Pettersson, S.; Spraul, M.; Schaefer, H.; Lawler, N. G.; Gray, N.; Whiley, L.; Nicholson, J. K. *J. Proteome Res.* **2021**, *20*, 3315−3329.
(39) Bizkarguenaga, M.; Bruzzone, C.; Gil-Redondo, R.; SanJuan, I.; Martin-Ruiz, I.; Barriales, D.; Palacios, A.; Pasco, S. T.; González-Valle, B.; Laín, A.; Herrera, L.; Azkarate, A.; Vesga, M. A.; Eguizabal, C.; Anguita, J.; Embade, N.; Mato, J. M.; Millet, O. *NMR Biomed.* **2022**, *35*, e4637−e4646.
(40) Liu, J.; Li, Z. B.; Lu, Q. Q.; Yu, Y.; Zhang, S. Q.; Ke, P. F.; Zhang, F.; Li, J. C. *Front. Immunol.* **2022**, *13*, 894170−894182.
(41) Danlos, F. X.; Grajeda-Iglesias, C.; Durand, S.; Sauvat, A.; Roumier, M.; Cantin, D.; Colomba, E.; Rohmer, J.; Pommeret, F.; Baciarello, G.; Willekens, C.; Vasse, M.; Griscelli, F.; Fahrner, J. E.; Goubet, A. G.; Dubuisson, A.; Derosa, L.; Nirmalathasan, N.; Bredel, D.; Mouraud, S.; Pradon, C.; Stoclin, A.; Rozenberg, F.; Duchemin, J.; Jourdi, G.; Ellouze, S.; Levavasseur, F.; Albigès, L.; Soria, J. C.; Barlesi, F.; Solary, E.; André, F.; Pène, F.; Ackerman, F.; Mouthon, L.;

https://doi.org/10.1021/acs.analchem.2c04514
Anal. Chem. 2023, 95, 3638−3646

Zitvogel, L.; Marabelle, A.; Michot, J. M.; Fontenay, M.; Kroemer, G. *Cell Death Dis.* **2021**, *12*, 258−268.
(42) Suvarna, K.; Salkar, A.; Palanivel, V.; Bankar, R.; Banerjee, N.; Gayathri J Pai, M. G. J.; Srivastava, A.; Singh, A.; Khatri, H.; Agrawal, S.; Shrivastav, O.; Shastri, J.; Srivastava, S. *J. Proteome Res.* **2021**, *20*, 4667−4680.
(43) Sindelar, M.; Stancliffe, E.; Schwaiger-Haber, M.; Anbukumar, D. S.; Adkins-Travis, K.; Goss, C. W.; O'Halloran, J. A.; Mudd, P. A.; Liu, W. C.; Albrecht, R. A.; García-Sastre, A.; Shriver, L. P.; Patti, G. J. *Cell Rep. Med.* **2021**, *2*, 100369−100389.
(44) Bahreini, M.; Hosseinzadegan, A.; Rashidi, A.; Miri, S. R.; Mirzaei, H. R.; Hajian, P. *Talanta* **2019**, *204*, 826−832.
(45) Rygula, A.; Majzner, K.; Marzec, K. M.; Kaczor, A.; Pilarczyk, M.; Baranska, M. *J. Raman Spectrosc.* **2013**, *44*, 1061−1076.
(46) Goulart, A. C. C.; Silveira, L.; Carvalho, H. C.; Dorta, C. B.; Pacheco, M. T. T.; Zângaro, R. A. *Lasers Med. Sci.* **2022**, *37*, 2217−2226.
(47) Shen, B.; Yi, X.; Sun, Y. T.; Bi, X. J.; Du, J. P.; Zhang, C.; Quan, S.; Zhang, F. F.; Sun, R.; Qian, L. J.; Ge, W. G.; Liu, W.; Liang, S.; Chen, H.; Zhang, Y.; Li, J.; Xu, J. Q.; He, Z. B.; Chen, B. F.; Wang, J.; Yan, H. X.; Zheng, Y. F.; Wang, D. L.; Zhu, J. S.; Kong, Z. Q.; Kang, Z. Y.; Liang, X.; Ding, X.; Ruan, G.; Xiang, N.; Cai, X.; Gao, H. H.; Li, L.; Li, S. N.; Xiao, Q.; Lu, T.; Zhu, Y.; Liu, H. F.; Chen, H. X.; Guo, T. N. *Cell* **2020**, *182*, 59−72.
(48) Chen, D. V. *Appl. Artif. Intell.* **2021**, *35*, 1147−1168.
(49) Luporini, R. L.; Pott-Junior, H.; Di Medeiros Leal, M. C. B.; Castro, A.; Ferreira, A. G.; Cominetti, M. R.; de Freitas Anibal, F. *Int. Immunopharmacol.* **2021**, *101*, 108313−108318.
(50) Nargis, H. F.; Nawaz, H.; Bhatti, H. N.; Jilani, K.; Saleem, M. *Spectrochim. Acta, Part A* **2021**, *246*, 119034−119042.

https://doi.org/10.1021/acs.analchem.2c04514
Anal. Chem. 2023, 95, 3638−3646